LASER INTERFEROMETER GRAVITATIONAL WAVE OBSERVATORY
- LIGO -
CALIFORNIA INSTITUTE OF TECHNOLOGY
MASSACHUSETTS INSTITUTE OF TECHNOLOGY

Technical Note **LIGO-T1800225–v2** 2018/10/30

Design and Testing of Composite Mirror Adaptive Optics

Aria Chaderjian
Mentors: Jon Richardson, Aidan Brooks

California Institute of Technology
LIGO Project, MS 18-34
Pasadena, CA 91125
Phone (626) 395-2129
Fax (626) 304-9834
E-mail: info@ligo.caltech.edu

Massachusetts Institute of Technology
LIGO Project, Room NW22-295
Cambridge, MA 02139
Phone (617) 253-4824
Fax (617) 253-7014
E-mail: info@ligo.mit.edu

LIGO Hanford Observatory
Route 10, Mile Marker 2
Richland, WA 99352
Phone (509) 372-8106
Fax (509) 372-8137
E-mail: info@ligo.caltech.edu

LIGO Livingston Observatory
19100 LIGO Lane
Livingston, LA 70754
Phone (225) 686-3100
Fax (225) 686-7189
E-mail: info@ligo.caltech.edu

http://www.ligo.caltech.edu/

1 Abstract

Adaptive optics work to reduce optical losses in the LIGO detectors, making them more sensitive to gravitational wave events. Mode-mismatch between the coupled optical cavities, caused by uncertainty in the radii of curvature and orientation of the interferometer optics, is one of the main sources of loss in Advanced LIGO. Thermal actuators are used to dynamically change the radius of curvature of certain interferometer optics, allowing mode mismatches to be reduced. Finely tunable astigmatic mirrors have the potential to be very useful in gravitational wave detectors for beam reflections at non-normal incidence, but have never been tested. These astigmatic composite mirrors are constructed by bonding a fused silica mirror to a non-axially-symmetric metal plate. When heated, the mirror is differentially distorted in the x- and y-directions due to its asymmetric design, resulting in an elliptical reflected beam profile. We model and test an initial mirror design, finding that it does, in fact, act as an astigmatic mirror. This finding opens a new avenue towards development of adaptive optics for current and next-generation gravitational wave detectors.

2 Text

Introduction

Gravitational waves were predicted in 1916 by Einstein's theory of general relativity, which holds that two objects orbiting one another in space will lose energy in the form of gravitational waves and gradually approach one another. These transverse waves propagate away from accelerating masses at the speed of light and contract and expand spacetime in their transverse planes. The expanded and contracted dimensions of space are orthogonal to each other, and oscillate every half-cycle of the gravitational wave. Through the detection of gravitational waves, scientists are able to observe the universe's most violent events, such as colliding black holes and supernovae billions of light years away. Observing such events allows for the study of the astrophysics of these extreme objects and their population statistics. Furthermore, the detected waveforms can be compared to predictions from relativity: a difference between the detected and predicted waveforms could indicate other currently unknown physical phenomena at work. The study of gravitational waves will also allow for discoveries in cosmology, such as enabling researchers to measure the current rate of cosmic expansion and how this rate has evolved.

The first, indirect, evidence for gravitational waves came in 1974 when Hulse and Taylor discovered a binary pair of pulsars (PSR B1913+16) 21,000 light years away from Earth. After tracking the radio emissions of one of the stars over several years, they determined that the time required for the stars to orbit one another was decreasing at the rate predicted by general relativity under the assumption that the stars were losing kinetic energy to gravitational waves. The first direct evidence for gravitational waves came in 2015, when each of the two Laser Interferometer Gravitational-Wave Observatory (LIGO) detectors directly detected the minuscule disturbances made to spacetime as the waves passed through the earth, confirming their existence. This first detection by LIGO came from the merging of two black holes. Since this first detection, other black hole mergers have been observed as well as an instance of a neutron star merger.

By the time gravitational waves reach LIGO, the waves distort spacetime by thousands of times smaller than the nucleus of an atom. For this reason, the laser interferometers used by LIGO to detect these waves must employ an unprecedented degree of precision. Adaptive optics works to make the detectors more sensitive by reducing optical losses, which can result from "scattering, reflections from optics, photo-detector quantum efficiency, and mismatches among cavities" [1]. Increased sensitivity will enable more astrophysical events to be detected.

Project Description

Mode-mismatch between cavities, caused by uncertainty in the radii of curvature and orientation of the optics of the interferometer, is one of the main sources of loss in Advanced LIGO. Thermal actuators change the radius of curvature of various optics to dynamically change the beam size, allowing mode mismatches to be reduced. Spherical actuators effectively correct mode-mismatch at normal incidence by changing the reflected beam size. At appreciable angles of incidence, however, an astigmatism is introduced, which changes the curvature of the reflected beam. This project seeks to design and build an astigmatic actuator to be used in such instances of non-normal incidence in order to spherically actuate on the beam.

Prior to designing and building an astigmatic actuator, a composite mirror spherical actuator was designed using finite element software and then built and tested in the lab. The spherical actuator was built by bonding a fused silica mirror 6mm thick to an aluminum disk 5mm thick, both with 25.4 mm diameters. The aluminum layer has a larger coefficient of thermal expansion than the silica mirror layer, so the back layer expands more than the front layer when heated, bending the front reflecting surface of the mirror as shown by Figure 1. The amount of heating can be tuned to precisely control the radius of curvature of the mirror and thereby control the focal distance of a reflected laser beam.

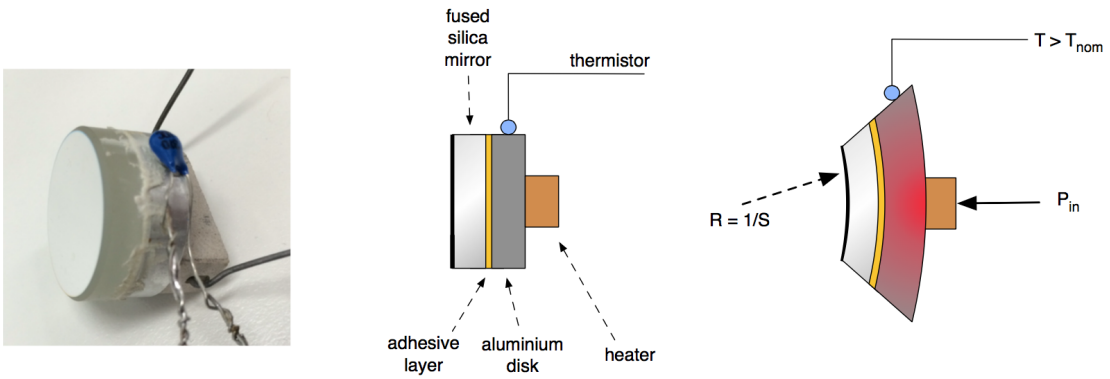

Figure 1: Example design of a composite mirror. The mirror is bonded to the aluminum disk with a vacuum-compatible adhesive. A thermistor is bonded to the Al disk to monitor the temperature, and a heater is bonded to the disk to provide heating. Image reproduced from [2].

Once testing confirmed that the composite mirror behaved as a spherical actuator, an astigmatic actuator was designed. This design was similar to the spherical actuator design but with portions along the y-axis of the aluminum disk removed to allow for differential expansion along the x- and y-axes, producing an astigmatic actuator.

Further data analysis is necessary to determine the angle of incidence at which this actuator will actuate spherically. Once this angle is determined, different geometries can be modeled and tested in order to be utilized at the specific angles of incidence required by LIGO. Other materials can also be investigated to produce a more reliable actuator.

3 Methods

Finite Element Modeling of Spherical Actuator

To determine an appropriate design for the composite mirror, various thicknesses, formations, and materials were modeled using finite element software. The optical path difference (OPD) and total displacement after heating 1 degree were recorded. Their ratio gives the coupling efficiency. For each thickness tested, the coupling efficiency was at least 0.968 (at r_{max}). Silica was tested as the mirror and aluminum was tested as the metal disk behind it. Copper was also tested as the metal disk but, as predicted, did not provide as much displacement because its coefficient of thermal expansion is less than that of aluminum.

Different radii were modeled for the aluminum disk, with the aluminum disk and silica mirror mounted concentrically. It was found that displacement of the front face of silica increases, seemingly in a linear fashion, as the aluminum radius increases. For practicality in the lab, since it would be difficult to adhere the silica to the aluminum of different radius in a concentric manner, aluminum disks of the same radius as the silica mirror were used.

The optical path difference for various thicknesses of silica and aluminum is shown in Figure 2. Silica thickness that is slightly more than twice the thickness of the aluminum backing is the optimal ratio for maximum OPD, but this ratio is not constant for various silica thicknesses. When the silica is thicker, maximum OPD occurs at a slightly higher ratio of silica thickness to aluminum thickness than it did for thinner silica thickness. For practicality of obtaining these thin disks, fused silica mirrors of thickness 6 mm and aluminum disks of thickness 5 mm were tested in the lab.

The defocus (S) was found using the equation for optical path difference (z), a function of radius (r) of a perfect spherical actuator:

$$z(r) = \frac{1}{2} S r^2. \tag{1}$$

Eq. 1 holds for a perfect spherical actuator. Other actuators have additional terms with increasing powers of r. To determine the residuals from approximating our actuator as a perfect spherical actuator, we subtract the OPD values obtained by the model from the OPD values of a perfect spherical actuator:

$$z_{spherical}(r) - z_{model}(r) = residual. \tag{2}$$

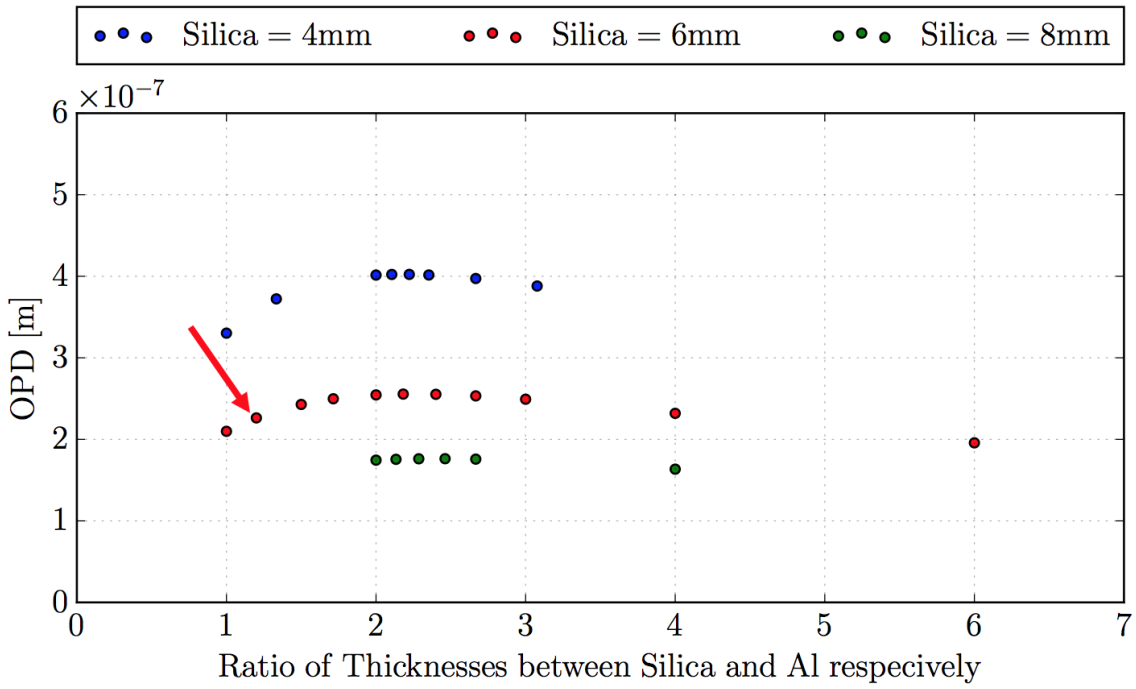

Figure 2: Predicted OPD at maximum radius for various thickness pairings for silica and aluminum disks. The red arrow points to the point corresponding to parameters tested in the lab.

For the thicknesses of fused silica and aluminum tested, 6 mm and 5mm respectively, the predicted OPD values obtained by the model, the OPD values of a perfect spherical actuator, and their difference as formulated by Eq. 2 are shown in Figure 3.

Optical Table Setup

A Hartmann Wavefront Sensor (HWS) was used to measure the effect of heating on a given mirror design. This device uses an array of apertures to divide an incoming wavefront into an array of smaller beams, each of which is focused into a CCD camera. A uniform, planar wavefront incident on the HWS will result in a regularly spaced grid of dots on the detector, while a distorted wavefront will result in an irregularly spaced grid of dots. These displaced dots can be used to calculate the shape of the wavefront, determining the spatial profile of the distorted mirror surface. Figure 4 shows the setup of the HWS on the optical table for this measurement.

Testing of Spherical Actuator

Simple composite mirrors were constructed by bonding a 6mm thick fused silica mirrors to a 5mm thick aluminum disk, each with 25.4 mm diameters. High temperature and low CTE epoxy (353NDPK) was used as the adhesive. Once the epoxy had cured for approximately 24 hours, an etched circuit heater was attached to the back of the aluminum disk and

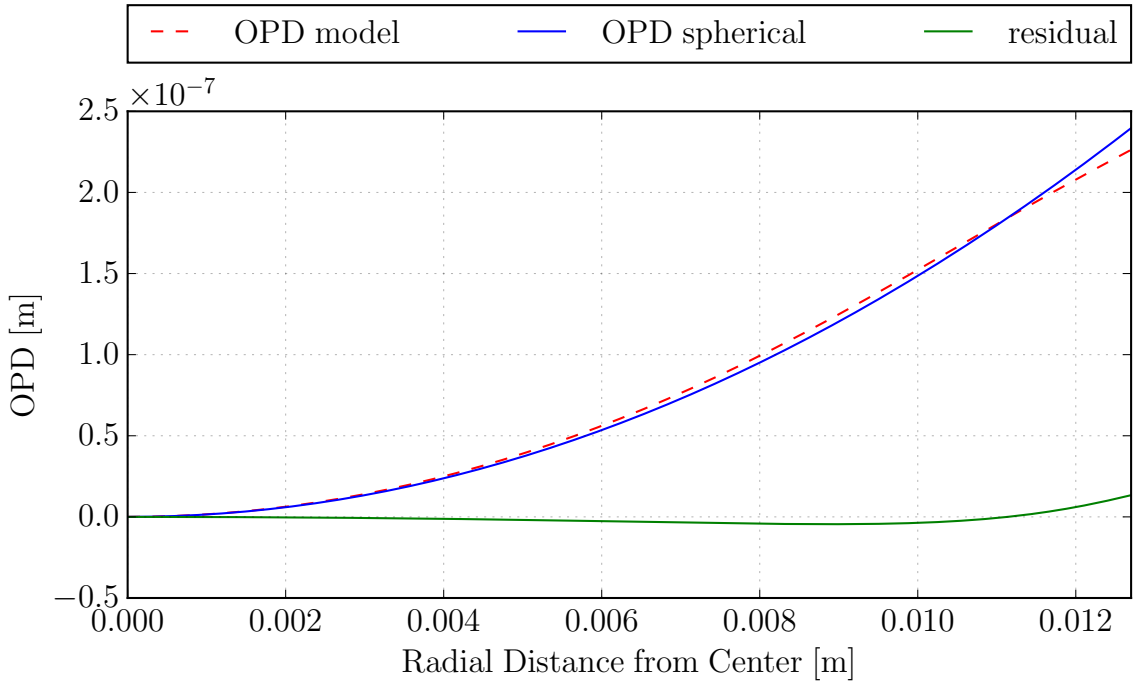

Figure 3: Best fit for OPD predicted by finite element modeling (OPD model), the corresponding data fit to the OPD of a perfect spherical actuator (OPD spherical), and their difference (residual). Note that residual is nearly zero, implying that a nearly perfect spherical actuator was modeled.

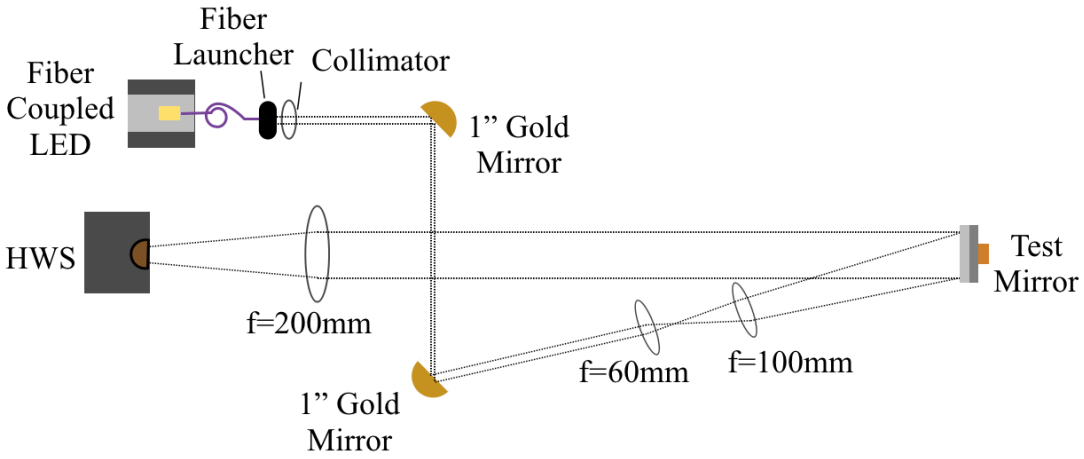

Figure 4: Test setup using a HWS to characterize the performance of an adaptive optic. A probe beam is reflected from the surface of the test mirror and focused onto the HWS. The difference in wavefront profile measured when the optic is hot versus cold provides the change in mirror surface profile.

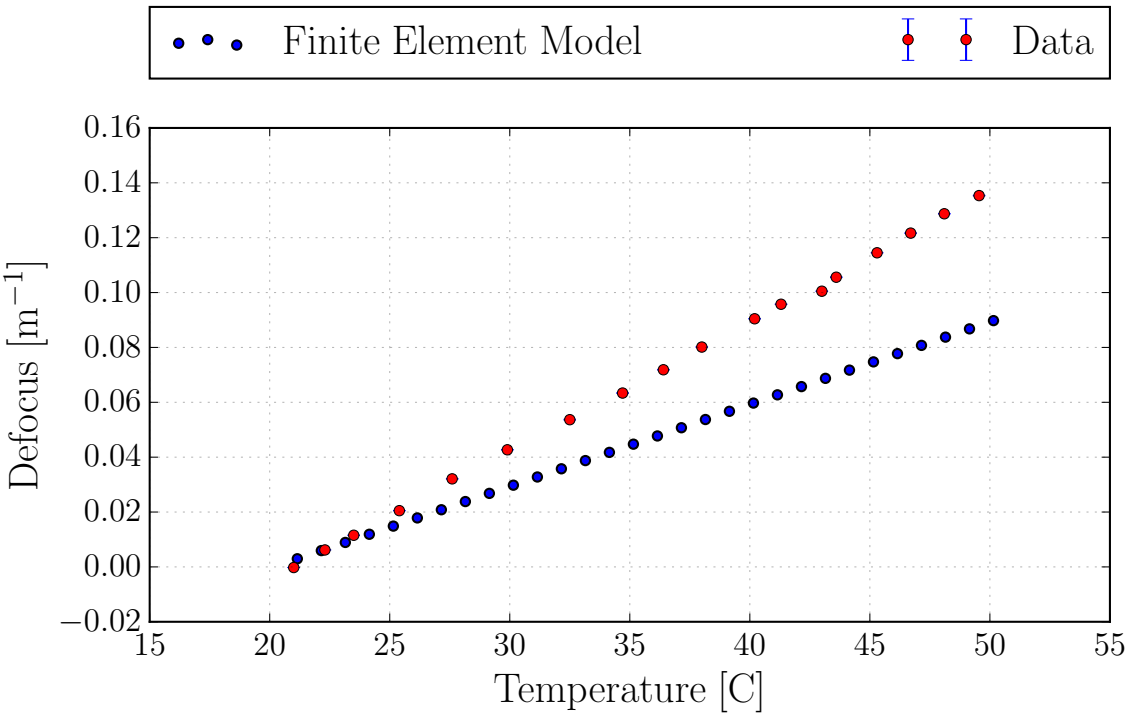

Figure 5: Various trials using the HWS to determine spherical power as temperature increases. Notice that both curves are linear with a positive slope. The two curves differ by a normalization factor of approximately 1.5, which is being investigated

connected to a power supply. A temperature sensor was connected to the heater; ideally, the temperature sensor would have been connected to the side of the aluminum disk, but the disk was too thin. This is a minimal problem, however, because the aluminum and fused silica are thermally conductive.

Using the power supply, the temperature of the composite mirror was increased from room temperature by increments of approximately 1.5 degrees to a final temperature of approximately 50 degrees C. Once temperature had stabilized, spherical power was recorded. As temperature increased, the spherical power increased. A phenomenon was sometimes observed in which the spherical power increased with heating until a point where spherical power dropped significantly despite temperature was still increasing. This drop in spherical power is currently believed to be the result of some release of mechanical stress.

The data collected from a single trial is shown in Figure 5 along with the predicted spherical power modeled using COMSOL. The model and the tested values differ by a normalization factor of approximately 1.5, which is being investigated. The linear trend implies a linear thermal actuator.

The wavefront map of this trial after heating 2.5 degrees is shown in Figure 6. This wavefront map was obtained by integrating the gradient field produced by the Hartmann sensor. The axially-symmetric wavefront map indicates that a spherical actuator was successfully constructed.

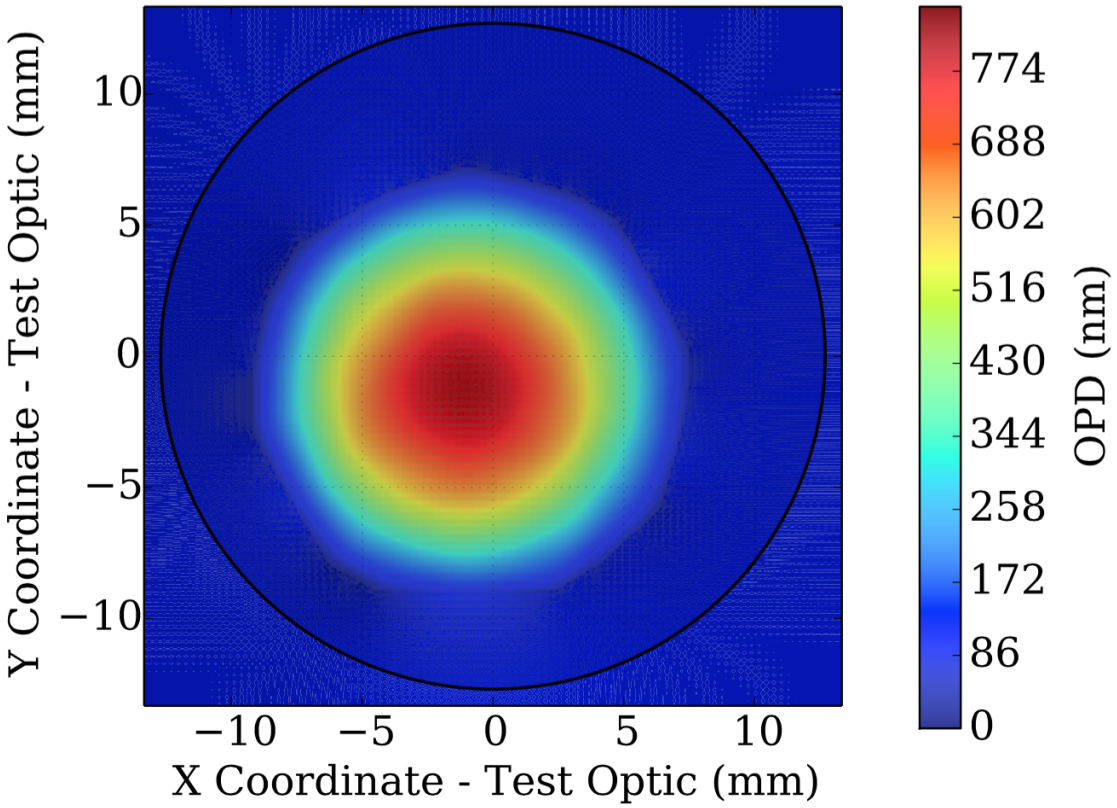

Figure 6: Wavefront map of simple composite mirror after 2.5 degrees heating. The axially-symmetric wavefront map indicates that a spherical actuator was constructed.

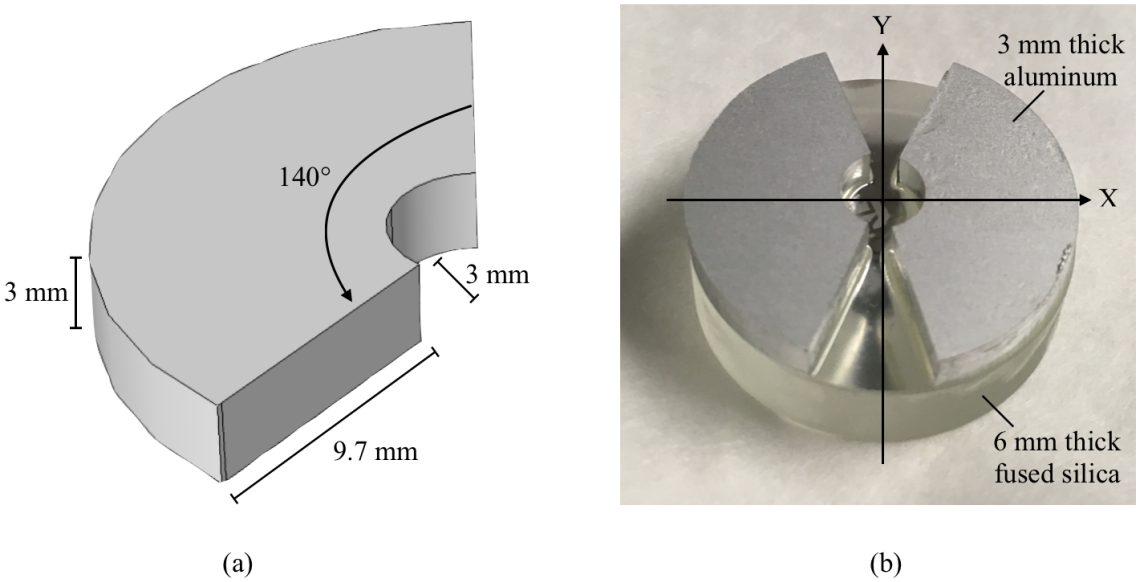

(a) (b)

Figure 7: (a) The design of each individual aluminum piece and (b) the astigmatic mirror.

Finite Element Modeling of Astigmatic Actuator

Finite element modeling determined that a viable design for an astigmatic mirror would involve segments of an aluminum disk with a circle of radius 3mm removed from the center. Two such segments would be bonded to the back of a silica mirror with 40 degrees of space between each segment. The design of each individual aluminum piece as well as the bonded mirror are shown in Figure 7.

This design was modeled to produce a defocus along the y-axis that is approximately 2.9 times the value of defocus along the x-axis as shown in Eq. 3, which would result in a significantly astigmatic mirror.

$$S_y = 2.866 S_x \tag{3}$$

The relation between astigmatism and the angle of incidence α at which the mirror would act as a spherical actuator is given by Eq. 4, derived from [7].

$$\frac{S_x}{S_y} = \cos^{-2}(\alpha) \tag{4}$$

In order to obtain a viable angle of incidence, this mirror should be rotated 90 degrees, effectively switching the x- and y-axes. This gives

$$\frac{S_x}{S_y} = 2.866. \tag{5}$$

Substituting the value for $\frac{S_x}{S_y}$ from Eq. 5 into Eq. 4 and solving for α gives

$$\alpha = 53.8 \tag{6}$$

which is an appropriate angle for implementing in aLIGO.

Testing of Astigmatic Actuator

The astigmatic actuator shown in Figure 7(b) was constructed using the same method as used for constructing the simple composite mirror. Care was taken to attach the etched circuit heater in a way as to equally span each aluminum piece. The thermistor was then attached to the heater.

The temperature of the mirror was increased from room temperature in increments of approximately 1.5 degrees and was allowed to stabilize at each increment.

The wavefront map obtained after heating the astigmatic actuator by 1.7 degrees is shown in Figure 8. The wavefront map reveals that there is more curvature in the beam along the y-axis than the x-axis, consistent with the prediction from modeling. At first glance, however, the wavefront map does not appear to show approximately 3-times more curvature along the y-axis as the x-axis as had been predicted by the model (see Eq. 3).

Data collected for the astigmatic mirror is still being analyzed. The pertinent parameters are cylindrical power which is the difference in defocus along the x- and y-directions, (Eq. 7), and spherical power which is the average defocus along the x- and y-directions (Eq. 8). General trends include the increase of cylindrical power with temperature and a seemingly non-existent relationship between spherical power and temperature.

$$C = S_y - S_x \tag{7}$$

$$S = \frac{1}{2}(S_x + S_y) \tag{8}$$

4 Future Work

In the future, the astigmatic actuator will be tested at the calculated angle of incidence to determine if it actuates spherically at that angle.

Other geometries and materials will be considered for the astigmatic mirror. Specifically, materials with lower mechanical hysteresis will be considered, as will materials such as calcium fluoride which would allow for UV bonding to be used instead of the epoxy. Designs which do not use any bonding agent at all can also be considered.

The fluctuations in spherical power persisting at stability of the astigmatic mirror as well as the sudden drops in spherical power sometimes observed when heating the simple composite mirrors should be characterized as well.

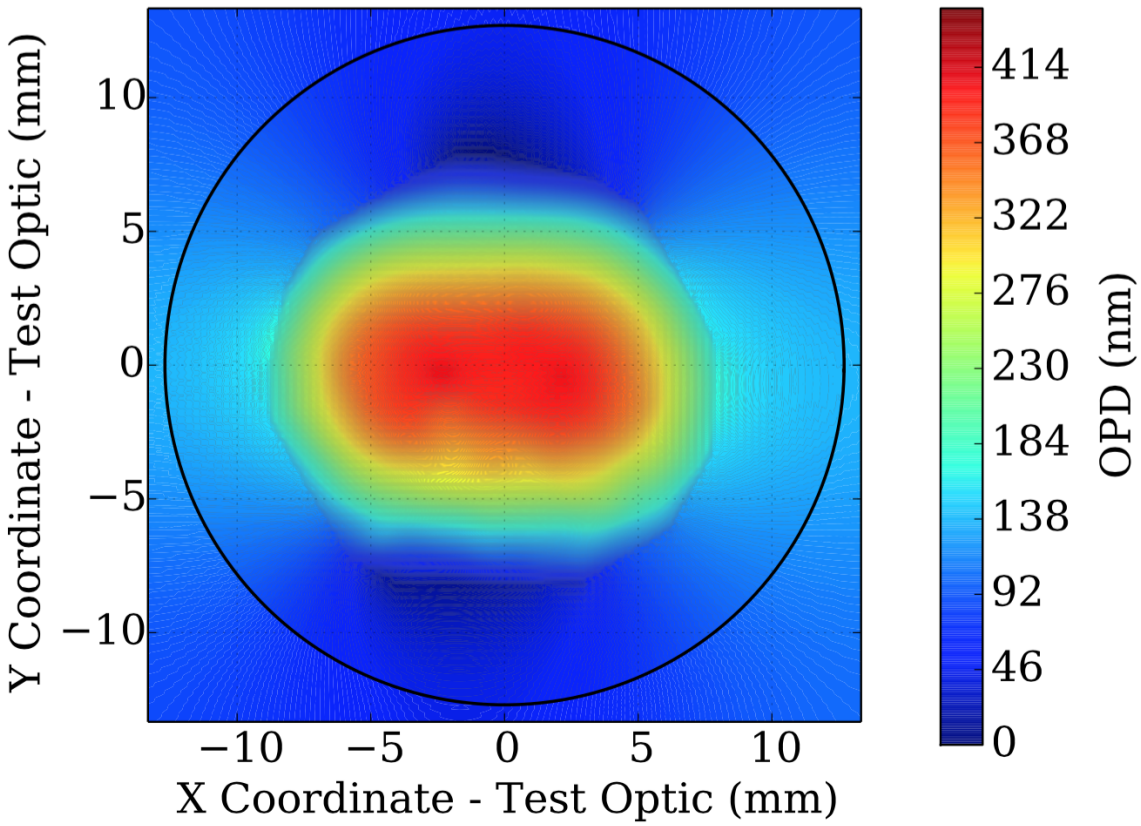

Figure 8: Wavefront map of astigmatic mirror after 1.7 degrees heating. Note that curvature in the beam changes more along the y-axis than along the x-axis.

References

[1] A. Perreca, et al., *Active wavefront control requirements and visualization for squeezing in Advanced LIGO and future gravitational wave detectors*, in prep.

[2] A. Brooks, private communication, 2018.

[3] H. Kogelnik and T. Li, *Laser Beams and Resonators*, 1966

[4] G. Fowles, *Introduction to Modern Optics*, 1975

[5] S. Timoshenko, *Analysis of Bi-Metal Thermostats*, 1925

[6] M.A. Arain, et al., *A Note on Optimal Spherical Approximation to Thermal Lensing*, 2006

[7] F.A. Jenkins and H.E. White, *Fundamentals of Optics*, 2001

[8] G.S. Monk, *Light Principles and Experiments*, 1937

5 Acknowledgements

I would like to sincerely thank Jon Richardson and Aidan Brooks for their guidance on this project. I would also like to thank Rana Adhikari and Koji Arai for their insights.

I am very grateful for the NSF REU funding and Caltech SFP funding that allowed me to have this research experience.